Supporting Information – A multi-scale model for the templated synthesis of mesoporous silica: The essential role of silica oligomers

Germán Pérez-Sánchez,[†,‡,¶] Szu-Chia Chien,[§,‖] José R. B. Gomes,[†] M. Natália D. S. Cordeiro,[‡] Scott M. Auerbach,[‖,⊥] Peter A. Monson,[‖] and Miguel Jorge[*,#,¶]

†*CICECO, Departamento de Química, Universidade de Aveiro, Campus Universitário de Santiago, 3810-193 Aveiro, Portugal*

‡*REQUIMTE, Department of Chemistry and Biochemistry, Faculty of Sciences, University of Porto, Rua Campo Alegre 687, 4169-007 Porto, Portugal*

¶*LSRE - Laboratory of Separation and Reaction Engineering - Associate Laboratory LSRE/LCM, Faculdade de Engenharia, Universidade do Porto, Rua Dr. Roberto Frias, 4200-465 Porto, Portugal*

§*Present address: Department of Materials Science and Engineering, Massachusetts Institute of Technology, Cambridge, Massachusetts 02139, USA*

‖*Department of Chemical Engineering, University of Massachusetts, 686 North Pleasant Street, Amherst, MA 01003-9303, USA*

⊥*Department of Chemistry, University of Massachusetts, 686 North Pleasant Street, Amherst, MA 01003-9303, USA*

#*Department of Chemical and Process Engineering, University of Strathclyde, 75 Montrose Street, Glasgow G1 1XJ, United Kingdom*

E-mail: miguel.jorge@strath.ac.uk

Phone: +44 (0)141 548 2825

Part I

Molecular models

In this paper, we extend the coarse-grained MARTINI force field[1] to systems containing silicate oligomers of different degrees of condensation. The MARTINI model is based on a mapping scheme whereby approximately four heavy (i.e., non-hydrogen) atoms are mapped onto one coarse-grained bead. As such, a single CG water bead represents four water molecules at the all-atom (AA) level. Details of the particular mapping used are provided below, together with tables of interaction parameters (Table S1 and S2). The MARTINI model has four

Table S 1 – Lennard-Jones parameter, ε, for the coarse-grained beads used in this work.

epsilon	Q_{SI}	P_4	BP_4	C_1	Q_0	Q_a	Q_{da}	SQ_{da}	SC_1
Q_{SI}	5.6(O)	4.5(II)	4.5(II)	3.5(IV)	4.5(II)	4.5(II)	4.5(II)	4.5(II)	3.5(IV)
P_4	4.5(II)	5.0(I)	5.6(O)	2.0(VIII)	5.6(O)	5.6(O)	5.6(O)	5.6(O)	2.0(VIII)
BP_4	4.5(II)	5.6(O)	5.0(I)	2.0(VIII)	5.6(O)	5.6(O)	5.6(O)	5.6(O)	2.0(VIII)
C_1	3.5(IV)	2.0(VIII)	2.0(VIII)	5.6(O)	2.0(IX)	2.0(IX)	2.0(IX)	2.0(IX)	3.5(IV)
Q_0	4.5(II)	5.6(O)	5.6(O)	2.0(IX)	3.5(IV)	4.5(II)	4.5(II)	4.5(II)	2.0(IX)
Q_a	4.5(II)	5.6(O)	5.6(O)	2.0(IX)	4.5(II)	5.0(I)	2.0(IX)	2.0(IX)	3.5(IV)
Q_{da}	4.5(II)	5.6(O)	5.6(O)	2.0(IX)	4.5(II)	2.0(IX)	5.6(O)	5.6(O)	2.0(IX)
SQ_{da}	4.5(II)	5.6(O)	5.6(O)	2.0(IX)	4.5(II)	2.0(IX)	5.6(O)	4.2	2.0(IX)
SC_1	3.5(IV)	2.0(IX)	2.0(IX)	3.5(IV)	2.0(IX)	3.5(IV)	2.0(IX)	2.0(IX)	2.62

The capital letters in parentheses denote the interaction levels according to the standard nomenclature of the MARTINI force-field. Units of ε are kJ/mol.

Table S 2 – σ values for the coarse-grained beads used in this work. Units of σ are in nm.

sigma	Q_{SI}	P_4	BP_4	C_1	Q_0	Q_a	Q_{da}	SQ_{da}	SC_1
Q_{SI}	0.47	0.47	0.47	0.47	0.47	0.47	0.47	0.47	0.47
P_4	0.47	0.47	0.47	0.47	0.47	0.47	0.47	0.47	0.47
BP_4	0.47	0.47	0.47	0.47	0.47	0.47	0.47	0.47	0.47
C_1	0.47	0.47	0.47	0.47	0.62	0.62	0.62	0.62	0.47
Q_0	0.47	0.47	0.47	0.62	0.47	0.47	0.47	0.47	0.62
Q_a	0.47	0.47	0.47	0.62	0.47	0.47	0.62	0.62	0.47
Q_{da}	0.47	0.47	0.47	0.62	0.47	0.62	0.47	0.47	0.62
SQ_{da}	0.47	0.47	0.47	0.62	0.47	0.62	0.47	0.43	0.62
SC_1	0.47	0.47	0.47	0.47	0.62	0.47	0.62	0.62	0.43

main types of interaction sites, namely polar (P), nonpolar (N), apolar (C) and charged (Q), with 18 subtypes overall. Q and N beads are subdivided taking into account their hydrogen-bonding capabilities: donor (d), acceptor (a), both (da) and none (0), whereas the degree of polarity in P and C beads is expressed by a number (from 1, low polarity, to 5, high polarity). A shifted Lennard-Jones (LJ) 12-6 potential energy function is used to describe the nonbonded interactions. The default effective bead size parameter is $\sigma = 0.47$ nm. This is assumed for each interaction pair except for the two special classes of rings and antifreeze particles (see below), as well as for interactions between charged Q beads and the most apolar types (C_1) and (C_2) beads, where the range of repulsion is extended by setting $\sigma = 0.62$ nm. The interaction strength is discretized in several levels, as follows: (O) 5.6; (I) 5.0; (II) 4.5; (III) 4.0; (IV) 3.5; (V) 3.1; (VI) 2.7; (VII); (VIII) 2.0 and (IX) 2.0 (with $\sigma =$ 0.62 nm), all of them in kJ/mol (more details can be consulted in ref.[1]). In addition to the LJ interaction, charged groups (type Q) interact via a shifted Coulombic potential energy function with a relative dielectric constant of 15. It should also be noted that the time scales of simulations using MARTINI should be rescaled by a factor of approximately four in order to reproduce realistic dynamic processes, because of the intrinsic speed-up caused by a reduction in the molecular degrees of freedom.[1] However, in this paper we have chosen not to apply this correction, so the reported times are simply the simulation times.

An important feature of MARTINI is the mapping of ring particles by prefixed "S" beads with the aim to preserve the geometry of small ring compounds. In this set, the effective interaction size σ is reduced to 0.43 rather than 0.47 nm, and the strength of ring-ring interactions ε is reduced to 75% of the original value. This allows ring particles to pack more closely together without freezing in order to reproduce the experimental liquid densities of small ring compounds.[1] Another challenging aspect of CG models is to accurately describe the behavior of water using a single LJ bead. In particular, a major concern is the unrealistic freezing of the CG model at temperatures above the melting temperature of real water. In order to overcome this, Marrink et al.[1] introduced antifreeze particles, (BP_4), which interact with all other particles in the system in exactly the same way as standard P_4 water beads. However, the σ value for interactions between BP_4 and P_4 is increased to 0.57 nm to disturb the lattice packing of the uniformly sized P_4 particles. This essentially amounts to adding an entropic penalty to the freezing transition, and brings the model into better agreement with real water behavior.

Following the MARTINI philosophy, we mapped our CTA^+ surfactant molecule using five beads, four C_1 for surfactant tails and Q_0 for the head. TMA^+ and solvated Br^- counterions were modeled by individual Q_a and Q_0 beads, respectively. Benzene molecules were described as three connected SC_1 beads, following the original MARTINI publication.[1] The surfactant model was validated against experimental data and AA simulation in previous papers by ourselves[2] and others.[3] Figure S1 shows the mapping used in this paper for non-silicate molecules.

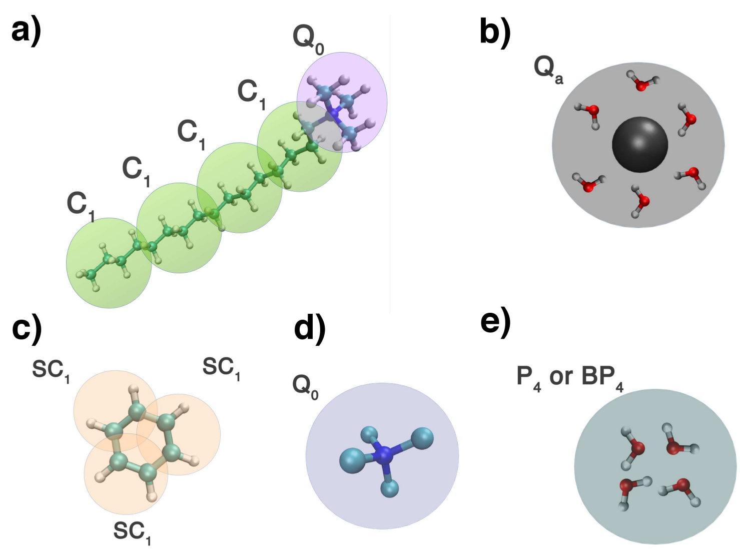

Figure S 1 – CG models for: (a) CTA^+ surfactant–four connected C_1 beads for surfactant tails (hydrophobic) joined with a charged Q_0 bead for the cationic surfactant head (hydrophilic) (b) one Q_a bead for bromide ions (Br^-) with the first hydration shell (c) three interconnected SC_1 beads for benzene (d) a single Q_0 bead for tetramethylammonium (TMA^+) cations (e) one bead for standard water molecules P_4 or antifreeze BP_4 particles, both with the 4:1 mapping.

To develop the CG force-field for silicates, we compared density profiles for both AA and CG models in preformed micelles containing silicates, to ensure that the correct physico-chemical behavior of each molecule was described at the CG level. The approach was described in detail in our previous paper,[2] where we also presented the model for silica monomers as a single Q_{SI} bead. In this paper, we calibrated the parameters for dimers and higher oligomers using the same procedure. In the end, linear silica oligomers were represented by connected Q_{da} beads (one for each Si-containing group), while cyclic silicates were described by SQ_{da} beads (again, one per Si atom). Figures S2 and S3 show the mapping of our CG model for the silicate molecules used in this work.

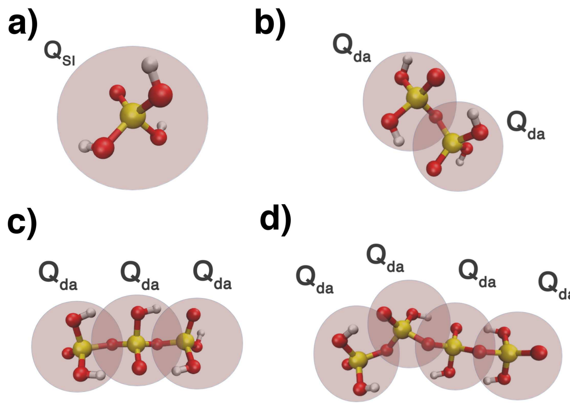

Figure S 2 – CG models for linear silicates: (a) monomer with one Q_{SI} bead (b) two connected Q_{da} beads for a dimer (c) three connected Q_{da} beads for a linear trimer (d) a linear tetramer with four Q_{da} connected beads.

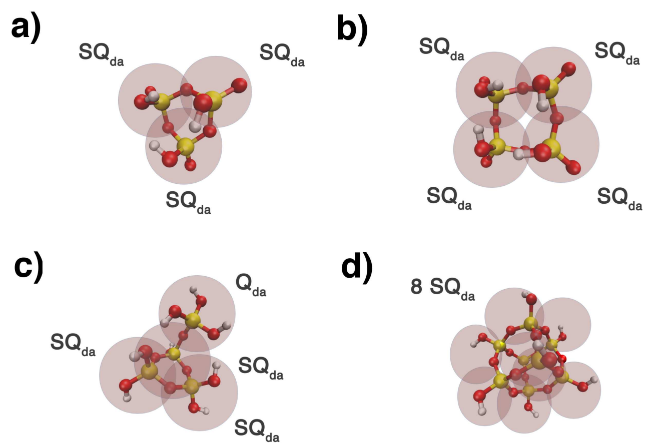

Figure S 3 – CG models for cyclic silicates: (a) three interconnected SQ_{da} beads for a cyclic trimer (b) a cyclic tetramer with four SQ_{da} interconnected beads (c) three interconnected SQ_{da} beads joined with one Q_{da} bead for branched cyclic tetramer (d) a double four ring (or cubic octamer) with eight SQ_{da} interconnected beads.

The comparison of density profiles between AA and CG models for silica dimers was shown in the main paper, but Figure S4 shows the (unsuccessful) comparison when the Q_{SI} potential parameters were transferred directly from monomers to dimers.

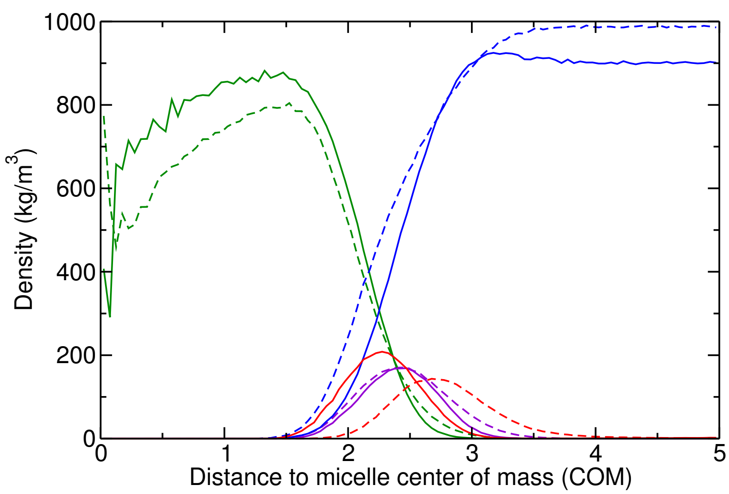

Figure S 4 – Density profile comparison, AA (dashed lines) and CG (solid lines), for the first attempt of silica dimers CG parameters using Q_{SI} parameters. Color code is as follows: Surfactant tails in green, surfactant heads in purple, water in blue and silicates in red.

In Figure S5 we show the comparisons for linear silicates (trimer and tetramer), while in Figure S6 we show the comparisons for cyclic silicates (trimer, tetramer, branched cyclic trimer and cubic octamer). In all cases, we obtained good agreement between the AA and CG profiles.

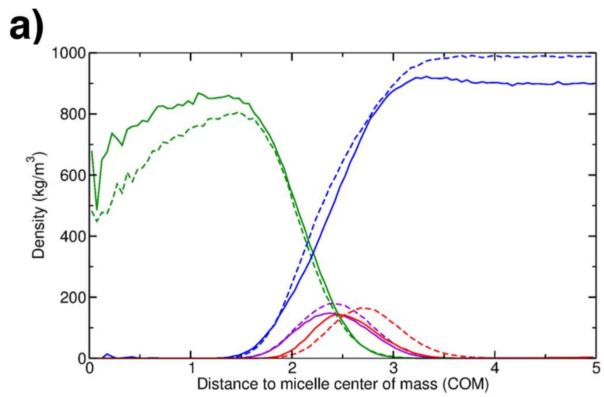

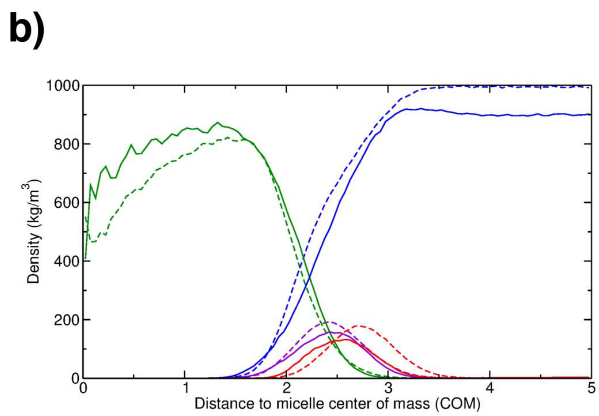

Figure S 5 – Density profile comparison, AA (dashed lines) and CG (solid lines), for (a) linear trimers and (b) linear tetramers, using the Q_{da} MARTINI parameters. Color code is the same as in Figure S4.

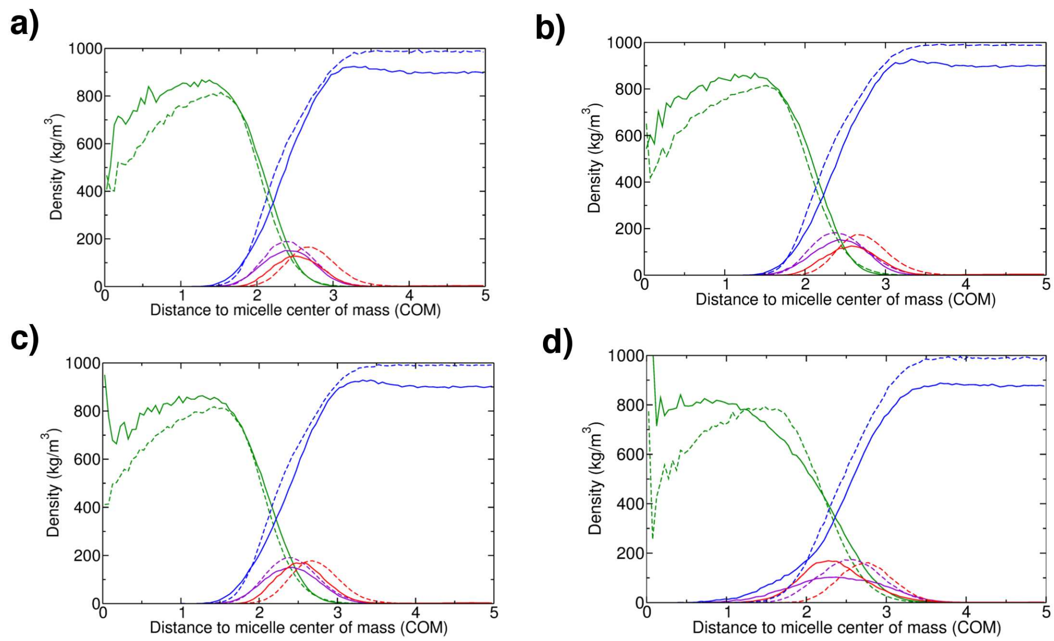

Figure S 6 – Density profile comparison, AA (dashed lines) and CG (solid lines), for (a) cyclic trimers, (b) cyclic tetramers, (c) branched cyclic trimers, and (d) double four ring octamers, using the SQ_{da} MARTINI parameters. Color code is the same as in Figure S4.

Part II

Additional Results

This section includes additional figures that are relevant for the discussion presented in the main paper. Figure S7 shows the detailed process of formation of a hexagonal mesophase starting from random distribution of silica dimers and surfactant. The system quickly formed small aggregates which fused into larger spherical micelles. No rod-like micelles were observed after this stage. Instead, micelles started to aggregate, changing their spherical shape into a more prolate shape. Several aggregates were formed in this way, which finally merged until the phase separation was complete. Finally, internal equilibration took place to yield an aggregate of small rod-like micelles similar to a HLC phase.

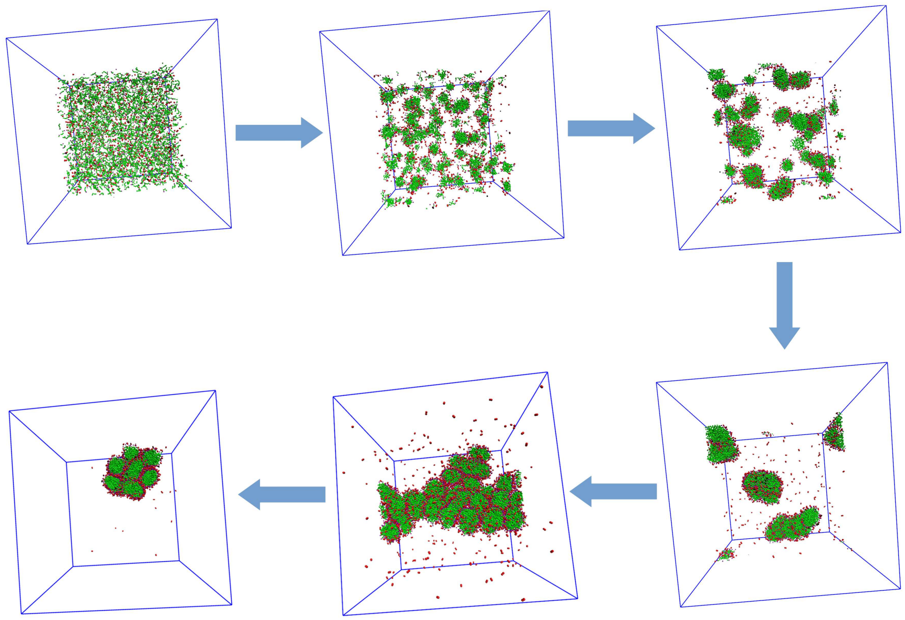

Figure S 7 – Diagram showing different stages of aggregation for a 6% w/w surfactant solution containing silicates in the form of 100% dimers, where all molecules were randomly placed at the beginning of the simulation. This corresponds to the results shown in Figure 2c of the main article. Color code is as follows: Surfactant tails in green, surfactant heads in purple, water in blue and silicates in red.

Figure S8 shows a simulation snapshot for a surfactant/water system with a mixture of 50% monomers/dimers.

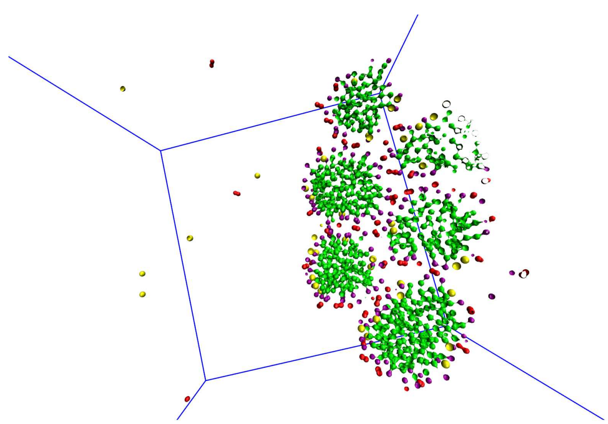

Figure S 8 – Snapshot showing a slice of the simulation box for the 50% monomer/dimer system. The slice is one-bead thick and the cutting plane was perpendicular to the main axis of the HLC mesostructure. Color code is as follows: Surfactant tails in green, surfactant heads in purple, water in blue, silica monomers in yellow and silica dimers in red.

We have cut out a slab with a thickness of one CG bead out of the HLC system to more clearly observe the core of the mesostructure. The figure shows the different role of silica monomers and dimers, with monomers well inside the rod surface whereas dimers are binding neighboring rods keeping the ordered structure. Several similar slices along the main axis of the HLC structure were taken, and in all of them the same pattern was found.

Firouzi et al.[4] showed that the addition of co-solvent molecules to an MCM-41 precursor solution induces a hexagonal-to-lamellar transition. Figure S9 shows the lamellar phase obtained after adding benzene molecules to a previously obtained hexagonal system (run 16) containing CTA^+ surfactants, water and silica dimers at 300K. It is clear to see how the benzene molecules are mainly placed in the hydrophobic core of the lamellar phase (Figure S9b).

With the aim to estimate the contribution of adding benzenes in the hexagonal-to-lamellar

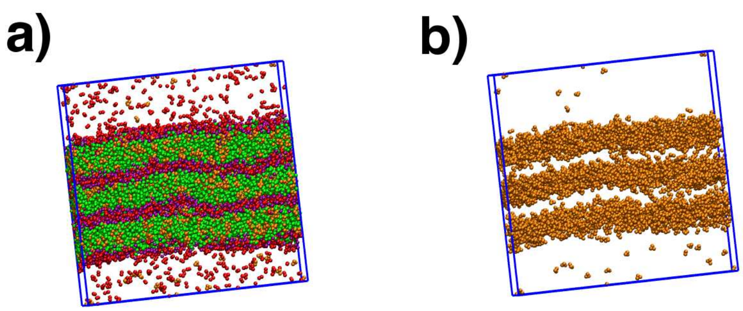

Figure S 9 – Lamellar phase obtained after a hexagonal-to-lamellar transition promoted by adding benzene (run 16): (a) snapshot with all of the components except water molecules (b) snapshot showing only benzene molecules to highlight their location in the hydrophobic core of the lamellar phase. Color code is as follows: Hydrophobic surfactant tails in green, hydrophilic surfactant heads in purple, silica dimers in red and benzenes in brown.

transition (Figure S9), we have calculated the hydrophobic surfactant volume in both hexagonal (before adding benzene) and lamellar phases (after benzene addition). In case of the hexagonal phase, we estimated the hydrophobic core volume by measuring the diameter and length of each rod (Figure S10).

We took different hydrophobic core rod sections along the main axis to obtain an average

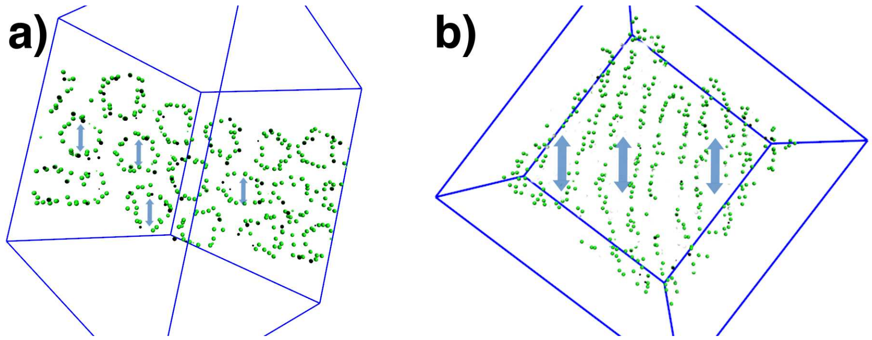

Figure S 10 – Rod diameters (a) and lengths (b) for the hexagonal system were visually obtained using the VMD[5] program. Only the external hydrophobic core beads in green color were plotted to facilitate the measurements. The system was split in different planes in order to enhance reading measurements.

diameter, and the hydrophobic core volume was obtained by multiplying each rod's cross-sectional area by its length. This led to a total volume of 2343 nm^3. In the case of the lamellar phase, we obtained the lamellae widths from the distance between the consecutive surfactant head density profile maximum. Then, to consider only the surfactant tail contribution we have subtracted the surfactant head bead size (0.47 nm). Afterwards, the hydrophobic core volume was obtained by multiplying the above width by three (3 lamellae) and by the area of the lamellae (box size is 20.38 nm). This yielded an approximate volume of 3564 nm^3. Subtracting the hydrophobic core volume of the hexagonal phase from that of the lamellar phase, we can say that the lamellar system is 1221 nm^3 larger than the hexagonal one. Values normalized by the total number of surfactant tails are provided in the main paper. On the other hand, the total volume of the added benzene molecules in the pure liquid phase was obtained by taking the density calculated by Marrink et al.[1] for the benzene MARTINI model (0.72 g/cm^3). In our HLC system, we added 3000 benzene particles so the volume contribution was 540 nm^3. This is significantly less than the effective volume increase during the transition.

Finally, Table S3 summarizes the number of components and the simulation box size which have been carried out in this work.

Table S 3 – Number of molecules and simulation box sizes at equilibrium for all the simulations carried out in this work.

	run 1	run 2	run 3	run 4	run 5	run 6	run 7	run 8	run 9	run 10	run 11	run 12	run 13	run 14	run 15	run 16	run 17
N_{Surf}	4000	4000	4000	4000	4000	2000	1800	1800	1000	999	1000	1000	1000	996	2000	4000	4000
N_{Br}	4000	-	-	-	-	-	-	-	-	-	-	-	-	-	2000	-	-
$N_W{}^*$	320K	240K	240K	240K	240K	120K	125K	125K	13K	13K	13K	13K	13K	13K	225K	34.5K	34.5K
N_{SI1}	-	4000	-	-	4000	1700	1200	600	-	-	-	-	-	-	256	-	-
N_{SI2}	-	-	2000	2000	-	150	300	600	500	-	-	-	-	-	-	2000	2000
N_{SI3R}	-	-	-	-	-	-	-	-	-	333	-	-	-	-	-	-	-
N_{SI4R}	-	-	-	-	-	-	-	-	-	-	250	-	-	-	-	-	-
N_{D4R}	-	-	-	-	-	-	-	-	-	-	-	125	250	166	768	-	-
N_{TMA}	-	-	-	-	-	-	-	-	-	-	-	-	-	-	4864	-	-
N_{BNZ}	-	-	-	-	-	-	-	-	-	-	-	-	-	-	-	3000	-
L_x	35.61	32.58	32.52	32.50	32.58	25.85	26.08	26.07	8.44	8.44	8.45	8.36	8.41	8.20	31.74	20.38	19.78
L_y	35.61	32.58	32.52	32.50	32.58	25.85	26.08	26.07	8.44	8.44	8.45	8.36	8.41	8.20	31.74	20.38	19.78
L_z	35.61	32.58	32.52	32.50	32.58	25.85	26.08	26.07	32.72	32.72	32.75	33.45	33.63	34.87	31.74	20.38	19.78

N_{Surf} number of surfactants; N_{Br} number of bromide ions; N_{SI1} number of silica monomers; N_W number of water molecules; N_{SI2} number of silica dimers; N_{SI3R} number of silica ring trimers; N_{SI4R} number of silica ring tetramers; N_{D4R} number of silica cubic octamers; N_{TMA} number of tetramethylammonium cations; N_{BNZ} number of benzene molecules; L_x, L_y and L_z box size in nanometers for x, y and z axis, respectively.

* K means 10^3.

References

(1) Marrink, S. J.; Risselada, H. J.; Yefimov, S.; Tieleman, D. P.; de Vries, A. H. The MARTINI Force Field: Coarse Grained Model for Biomolecular Simulations. *J. Phys. Chem. B* **2007**, *111*, 7812–7824.

(2) Pérez-Sánchez, G.; Gomes, J. R. B.; Jorge, M. Modeling Self-Assembly of Silica/Surfactant Mesostructures in the Templated Synthesis of Nanoporous Solids. *Langmuir* **2013**, *29*, 2387–2396.

(3) Wu, R.; Deng, M.; Kong, B.; Yang, X. Coarse-Grained Molecular Dynamics Simulation of Ammonium Surfactant Self-Assemblies: Micelles and Vesicles. *J. Phys. Chem. B* **2009**, *113*, 15010–15016.

(4) Firouzi, A.; Atef, F.; Oertli, A. G.; Stucky, G. D.; Chmelka, B. F. Alkaline Lyotropic Silicate-Surfactant Liquid Crystals. *J. Am. Chem. Soc.* **1997**, *119*, 3596–3610.

(5) Humphrey, W.; Dalke, A.; Schulten, K. VMD – Visual Molecular Dynamics. *J. Molec. Graphics* **1996**, *14*, 33–38.